Mar. 2013, Volume 7, No. 3 (Serial No. 64), pp. 261-272
Journal of Civil Engineering and Architecture, ISSN 1934-7359, USA

Penetration of the Stiffener Web to Deck Plate Weld in Orthotropic Plated Bridge Decks

Hans De Backer, Amelie Outtier and Philippe Van Bogaert
Department of Civil Engineering, Ghent University, Ghent B-9052, Belgium

Abstract: This paper reports the results of experimental research concerning the connection between the deck plate and the web of the longitudinal stiffeners in an orthotropic plated bridge deck on a microscopic scale. An important number of test specimens of a weld are studied with the help of a video microscope, to detect the efficiency of the root of the weld. The second part of the paper is concerned with parametric analysis of the lack of weld penetration by using accurate finite element modelling. The results demonstrate that the weld quality often required can not always be assured, which surely has important consequence on the stresses in the weld and the fatigue resistance.

Key words: Weld penetration, orthotropic plated bridge deck, stiffener web to deck plate weld.

1. Introduction

Orthotropic plated steel bridge decks are frequently used for large span bridges, because of the slenderness and lightness of the deck concept, as well as because of their contribution to the global resistance and durability of the bridge structure. Hence, eight out of the 10 largest suspension bridges in the world use the orthotropic deck concept. In addition, the capacity of the orthotropic plated deck concept allows for the design of slender structures as for example tied arch bridges for railway bridges with a structural depth of 1 m only and spanning more than 130 m. The design practice in Belgium has profoundly demonstrated this capacity [1-3], mainly in the case of the development of the Belgian section of the European network of high speed lines where a considerable number of short to medium span bridges for the high-speed railway lines were built, including some orthotropic decks. All practical examples and geometries used in this paper are linked to one of these bridges, the bridge crossing the Albert Canal in the city of Antwerp [4, 5].

However, orthotropic plated bridge decks are highly sensitive to fatigue damage, requiring in-depth fatigue analysis (EN1993-1-1 and EN1993-2 [6, 7]), to assure the fulfilment of various fatigue criterions. The stresses caused by traffic load on the bridge deck show severe concentrations and rapid changes of the large amplitudes. This subject has been studied extensively [1, 5, 8,]. One of the determining factors in the development of fatigue cracks is the weld quality which is closely linked with the degree of weld penetration. This is especially true when looking at the fatigue detail existing at the weld between the web of the longitudinal stiffeners and the deck plate [9, 10]. The focal point in this paper is the assessment on microscopic scale of a considerable number of weld connections, used for the stiffener web to deck plate fatigue detail, which were constructed by various steel fabricators. Subsequently, these results are compared with detailed finite element calculations of the fatigue detail under consideration.

2. Experimental Setup

A number of test specimens, independently manufactured by three different Belgian steel fabricators according to identical welding parameters, were gathered for this research. An overview of the

Corresponding author: Hans De Backer, Dr., professor, research fields: bridge, tunnel and road engineering. E-mail: Hans.DeBacker@UGent.be.

distribution of the test specimens is given in Table 1. The choice for more than one fabricator is made to ensure that the test batch is built up as homogeneous as possible. While the majority of specimens originate from one fabricator, possible structural errors caused by his specific production method can be checked for by comparing the results with those from two other fabricators. All test specimens of all fabricators were accepted to be a fair representation of the state-of-the-art for this specific weld in Europe, using partial penetration welds with a weld penetration of at least 80%.

The dimensions of the specimens are quite similar to those of the bridge across the Albert Canal in Antwerp, Belgium. This bridge is considered to be a relevant example for medium span orthotropic plated railway bridges in Europe. An 8 mm thick plate, steel quality S235 J2 G4-C, representing the web of the trapezoidal longitudinal stiffeners, is welded to the deck plate, steel quality S235 J2 G4, which has a thickness varying from 12 mm to 18 mm, along an angle of 81.79^{o}. This makes it representative for a trapezoidal stiffener with a top width of 300 mm, a bottom width of 200 mm and a stiffener height of 350 mm, which are quite common dimensions for orthotropic plated bridge decks. Identical welding procedure specifications were used as on a number of recently built orthotropic plated bridge decks. These procedures were certified by the Belgian Welding Institute for internal use. Before testing, the specimens are cut in strips, with a thickness of 25-50 mm each. The width of the constitutive plates of the specimens varies depending on the fabricator between 50 mm and 300 mm. Fig. 1 shows the necessary weld preparation as well as the resulting weld for the test specimen. The weld penetration that is displayed concerns the minimum penetration that needs to be guaranteed by the fabricators, with a full penetration weld being the obvious maximum.

To study the welds, a video microscope by courtesy of the Magnel Laboratory of Ghent University could be used. The digital microscope which was used for this research is a video-inspection tool with a high resolution, of which the camera, combined with a light source, is mounted on a flexible probe, which is equipped with a zoom lens allowing for magnification factors between 35 and 210. The apparatus was mounted on a stand, since the lens does not allow for auto focus, which slightly complicates the focusing. The latter was done manually, as shown in Fig. 2.

3. Classification of the Different Weld Types

All photographs allow for measuring the size and shape of the lack of weld penetration appearing at the backside of the considered weld. To allow for cataloguing the photographs, the 126 images of both sides of each test specimen can be divided into five different weld types. This division can be done using two different geometric parameters: the depth *d*, of the lack of weld penetration and the fillet diameter 2*R*, of the root of the lack of weld penetration.

The depth, *d*, is measured horizontally along an axis which is vertically situated in the middle of the lack of weld penetration. The origin of this axis coincides with the intersection of the axis of the lack of weld penetration with the virtual extension of the edge of the stiffener web. The axis' orientation is pointed to the outside of the trapezoidal closed stiffener. This

Table 1 Composition of the test specimens.

	Number of test specimens
Fabricator 1	55
Fabricator 2	4
Fabricator 3	4

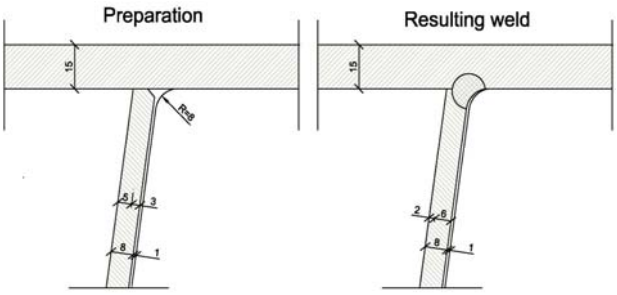

Fig. 1 Partial penetration weld of the test specimen.

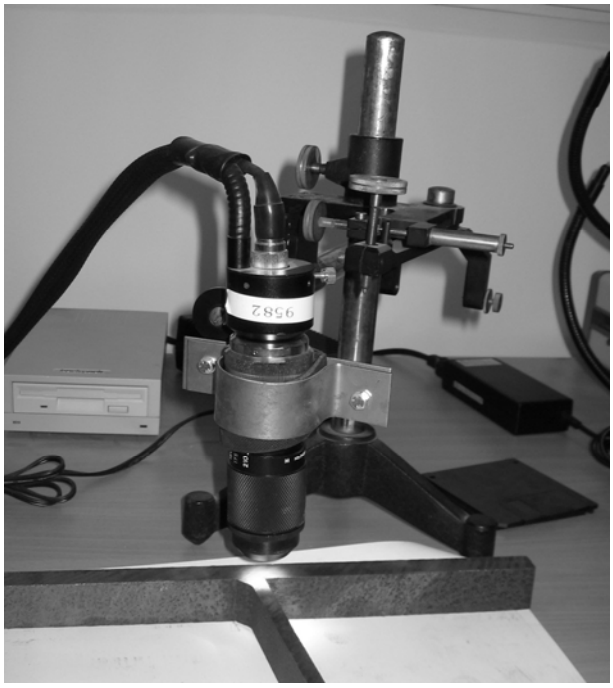

Fig. 2 Test specimen being studied using video microscope.

implies that positive values of d correspond with a large lack of weld penetration and negative values with the opposite, being an excessive use of weld material. To describe the curvature of the lack of weld penetration, a second parameter, 2*R*, is used, defined as the diameter of the cavity perimeter for positive values of *d* and as the radius of the rounding of the weld root from excess weld material, for negative values of *d*.

These two geometric parameters define five different weld types:

(1) "Type A": These specimens are characterized by a lack of weld penetration in the truest sense of the word, as shown in Fig. 3. They all satisfy the following two conditions for the geometric parameters:

$$d > 0 \quad (1)$$

$$|d| > 2R \quad (2)$$

The cavity at the back of the weld is deeper than its width. It is important to bear in mind that the parameter 2*R* needs to be seen as the width of the lack of weld penetration, since the end of the cavity is no perfect circle. At best, this parameter is the diameter of the virtual circle close to the cavity perimeter. A photograph of such a weld is shown in Fig. 4a;

(2) "Type B": The second group of weld details contains all specimens which settle the following two equations, as shown in Fig. 3:

$$d > 0 \quad (3)$$

$$|d| \le 2R \quad (4)$$

Since *d* is positive, this weld type still concerns a true lack of weld penetration, although its size is considerably smaller than for "Type A". A typical example of "Type B" is given in the photograph in Fig. 4b;

(3) "Type C": This weld class groups all specimens where virtually no lack of weld penetration exists. The

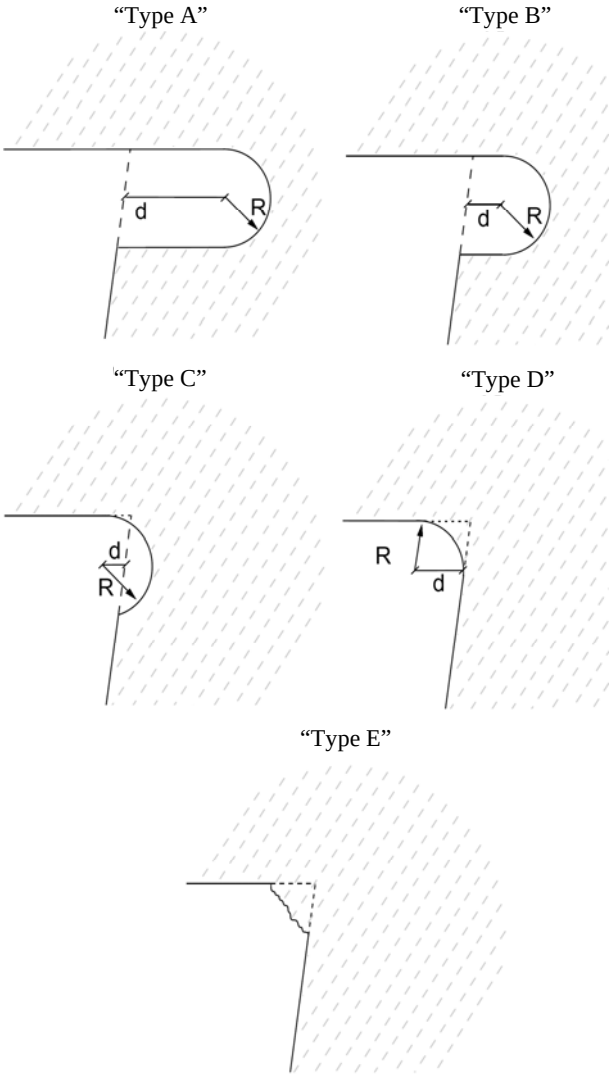

Fig. 3 Weld classification.

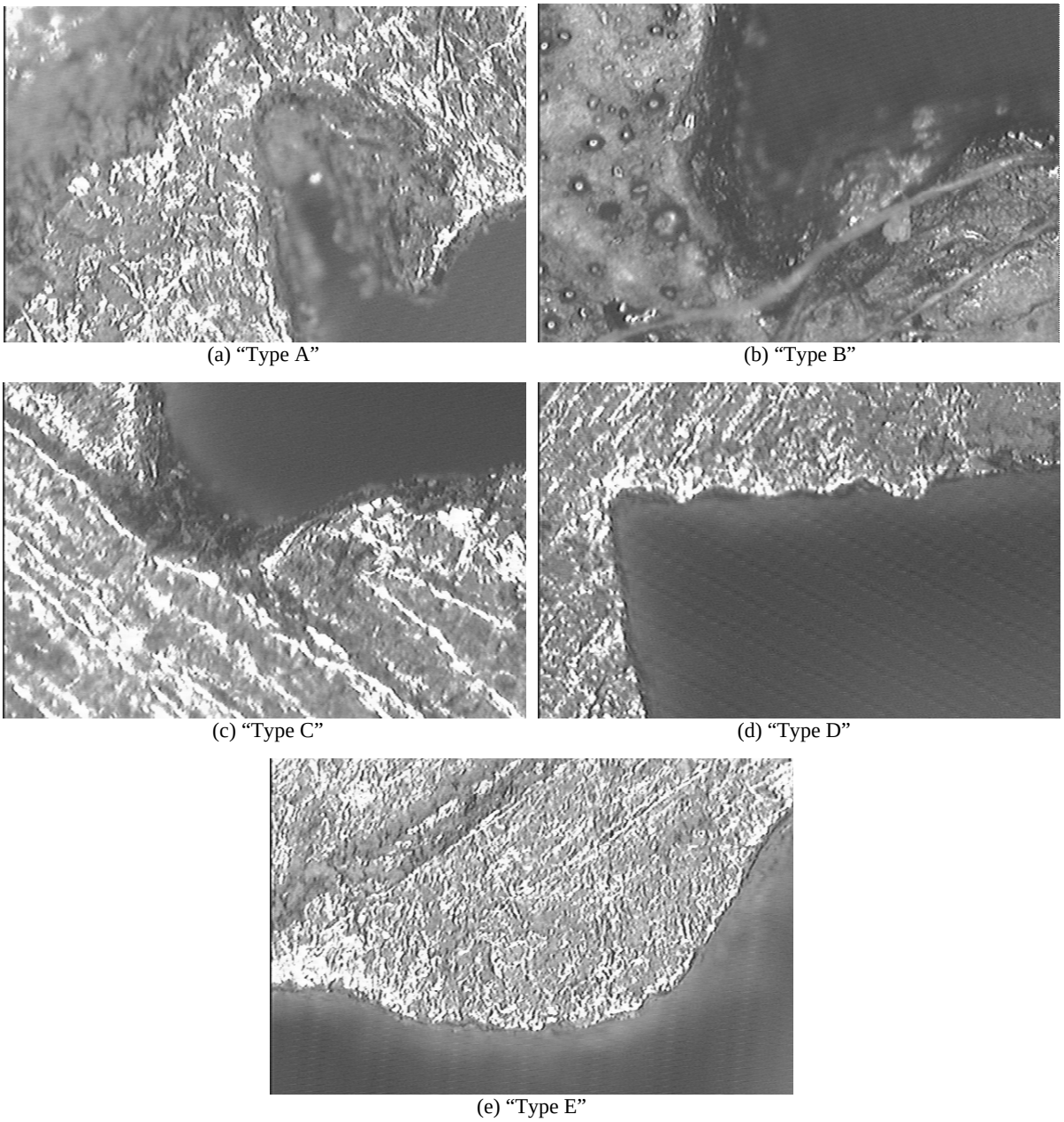

(a) “Type A” (b) “Type B”

(c) “Type C” (d) “Type D”

(e) “Type E”

Fig. 4 Microscopic images of the lack of weld penetration for the different weld types.

back of the weld can be considered as a small cavity at most. From this weld type on, the depth of all weld types becomes negative, as is shown in Fig. 3.

$$d \le 0 \tag{5}$$

$$|d| < R \tag{6}$$

Fig. 4c shows a characteristic example of a weld of “Type C”;

(4) “Type D”: The next weld type distinguishes itself by a weld ending which in fact forms a rounding of the connection between stiffener web and deck plate, as illustrated in Fig. 4d. All of these specimens comply with the notations as defined in Fig. 3, the following formulas show:

$$d \le 0 \tag{7}$$

$$|d| \ge R \tag{8}$$

(5) “Type E”: Finally, “Type E” forms the remaining weld category. This weld type groups all of the specimens which can not be catalogued in the

previous types. Most are characterized by excessive weld penetrations as shown in Fig. 4e. This weld type is not being considered in the finite element models of the following paragraphs.

The subdivision of all specimens in different types is summarised in Table 2 which lists the numbers of occurrence of each weld type for each fabricator separately. Tables 3 and 4 list the average, as well as the minimal and maximal value, for the geometrical parameters 2*R* and *d* for each weld type.

"Type C" and to a lesser extent "Type B" are the most common weld types in this limited batch. Also, there appears to be a slightly different distribution of the specimens over the five weld types for the three different steel fabricators. However, one of the two smaller batches delivers results comparable to the specimens manufactured by the first fabricator, indicating that this distribution might represent the actual distribution of weld types in orthotropic plated bridge decks. Clearly, for the third batch "Type A" is dominant. Nevertheless, it is immediately obvious that only a small part of the specimens, meets the initial objective, being a weld penetration between 80% and 100%.

Table 2 Number of tested specimens of each weld type.

	"Type A"	"Type B"	"Type C"	"Type D"	"Type E"
Fabricator 1					
Number	10	26	49	15	10
Percentage	9	24	44	14	9
Fabricator 2					
Number	1	2	4	0	1
Percentage	13	25	50	0	13
Fabricator 3					
Number	5	1	1	1	0
Percentage	63	13	13	13	0
Total					
Number	16	29	54	16	11
Percentage	13	23	42	13	9

Table 3 Summary of the diameters 2*R* of the lack of weld penetration.

(mm)	"Type A"	"Type B"	"Type C"	"Type D"
Average	0.22	0.43	0.49	0.32
Maximum	0.49	1.06	1.61	0.66
Minimum	0.06	0.13	0.05	0.11

Table 4 Summary of the depths *d* of the lack of weld penetration.

(mm)	"Type A"	"Type B"	"Type C"	"Type D"
Average	0.59	0.14	-0.14	-0.19
Maximum	2.06	0.46	-0.01	-0.05
Minimum	0.10	0.004	-0.78	-0.33

As expected, the specimens of "Type A" have the smallest diameters, since the stiffeners are pushed against the deck plate during welding. As the weld material reaches further into the narrow cavity between the steel plates, evolving from "Type A" to "Type B" and further on, and as *d* becomes smaller and finally negative, the diameter increases. Where the diameter needs to be interpreted for a "Type A"-weld as the width of the lack of weld penetration, for a "Type D"-weld it becomes the curvature of the fillet between the two plates of the orthotropic decking. Moreover, 2*R* is a generalisation of the cavity fillet, since actually, the weld end is an approximation of a circular segment drawn through the real circumference of the weld edge, as can be seen in the illustrations in Fig. 4.

4. Finite Element Modelling of the Weld Connecting the Stiffener Web and the Deck Plate

In order to assess the influence of the geometry of the aforementioned various weld types on the stresses appearing in the stiffener web to deck plate connection, a detailed finite element model was developed. This detailed model uses more than 250,000 three-dimensional elements to simulate only a part of this connection only instead of an entire orthotropic plated bridge deck. Accurate simulation of a whole deck using three-dimensional elements would have required to represent all steel plates of the deck by at least four or five layers of volume elements. The complexity of such a model requires computer memory in excess of standard processors. Since such

hardware was not available, a more adequate calculation strategy was followed.

The part of the bridge deck surrounding the considered weld is simulated through a volume element with 100 mm width, as shown in Fig. 5. In the longitudinal direction, a segment length of 200 mm is used, representing a section of central part of the orthotropic plated bridge deck between two consecutive crossbeams.

The problem of assessing the correct boundary conditions of such a fractional part of an entire bridge deck forms the Achilles heel of the calculation method. After all, the development of a highly sophisticated finite element model can be justly questioned if there is a reasonable doubt concerning the validity of the boundary conditions representing the influence of the remaining part of the orthotropic plated bridge deck derived from an overly simplified finite element model or from very basic analytical calculations.

Because of this, the calculation strategy is based on an inverse application of the superelement theory and implemented in the finite element software SAMCEF, produced by LMS Samtech. The superelement theory was developed to allow users of finite element software to model more complex structures. In order to reduce processor time and memory usage, the theory uses the results of totally independent calculations of a detail of the structure to calculate the behaviour of the structure as a whole. In the present case, it proved more useful to use the theory in its inverse form, i.e., to use a model of the entire structure to determine the boundary conditions to be imposed on the detailed model of the weld.

To allow for this, the global finite element model represents two consecutive sections of an orthotropic plated bridge deck, including the main girders and three crossbeams. The model uses two-dimensional shell elements and is displayed in Fig. 6. The element sizes allow determination in a precise manner of the very concentrated stress peaks in the welds of the orthotropic plated deck. However, since only

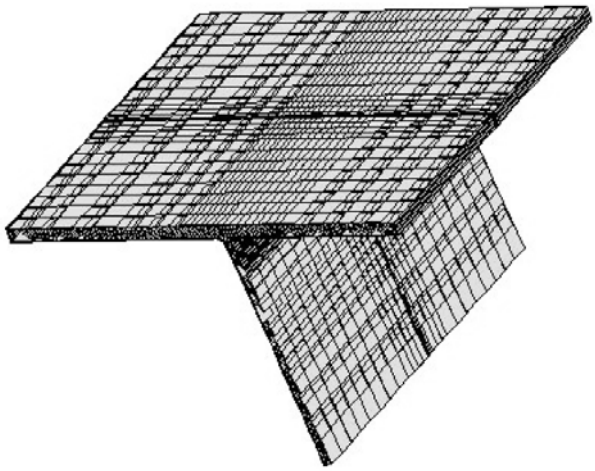

Fig. 5 Detailed finite element model of the stiffener web to deck plate connection.

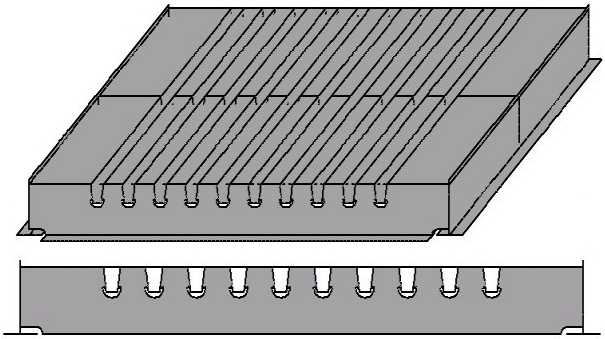

Fig. 6 Finite element model of an orthotropic plated bridge deck.

two-dimensional elements are used, this model does not immediately allow to comply with the volume-elements, needed to assess the influence of the weld penetration. Still, the model is sufficiently accurate to determine the boundary conditions existing at the edges of the detailed model. The procedure then comprises the following steps:

(1) The full scale model is calculated first;

(2) All displacement components, displacements as well as rotations of the edges of the detailed model are determined;

(3) These six components of the displacements are imposed on the detailed model as prescribed displacements;

(4) The detailed model can be calculated, without using any further boundary conditions or fixations, since the displacements of the full scale model directly

guarantee the equilibrium of external actions.

During the third step of this procedure, imposing displacement components to the median of each two-dimensional edge surface of the detailed model is to be avoided. Instead, these displacements are to be mapped across the entire surface. Should the procedure fail to do this, the prescribed displacements would be enforced in a very localised area resulting in serious abnormal situations during the calculation of the detailed model. Especially rotations would be seriously triggered. Furthermore, it is necessary to translate the six translation models in a way that leads to correct results in the detailed model. Hence, rotations of the deck plate must be imposed on the two-dimensional sides of the detailed model as translations resulting in the same rotation of the volume elements as derived from the plate elements of the full scale model.

While using finite element models of such complexity, the meshing must be as smooth and detailed as possible. This is necessary because it has been documented that the element size and distribution can slightly influence the size of hotspot stresses calculated using finite element software resulting in higher stresses then are to be expected [11]. Hence, all finite element models used during the research phase use similar mesh distributions, to allow for comparison of the results of various physical sample cases. If the meshes are comparable, possible trends becoming apparent when comparing the results of a parametric analysis can still be accepted. Nevertheless, it is recommended to read all simulation results more in qualitative fashion than strictly quantitative.

5. Comparison of Samples with Finite Element Modelling

The various weld types, as discussed in Section 3, have been simulated by using the detailed finite element model according to the dimensions in Tables 3 and 4. The dimensions of the bridge deck are those of the recently built bridge deck across the Albert Canal as mentioned before. To allow for a comparison, the various weld types are all loaded by a wheel print of 300 mm × 300 mm and subjected to a vertical uniform pressure of 0.53 MPa. This value corresponds to the maximum wheel load of a construction site lorry of 45,000 kg mass, which is the heaviest regular vehicle load allowed in Belgium. The wheel print is located adjacent to the web of the second longitudinal stiffener in the field between the first two trapezoidal stiffeners.

Due to the sensitivities of the finite element models described in the previous paragraph, the results in Fig. 7 need to be interpreted qualitatively more than quantitatively. This figure clearly illustrates that both the absolute size and the location of the stress peak differs for the four weld types being considered. As the weld evolves from “Type A” to “Type C”, the location of the stress peak starts moving in the direction of the deck plate, while decreasing slightly in value. “Type D” on the other hand, which has no real lack of weld penetration, is characterized by an obvious rise of stresses. It looks as if the stress peak for this specific weld type is located where the cavity has its largest curvature. To allow for a more detailed study of this phenomenon, a parametric analysis is performed, which is described in the following paragraph.

6. Parametric Study

The value of d/R can be looked at as being directly linked to the size and the shape of the lack of weld penetration, whereas $2R$ must be considered more as a scale factor. Hence, the parameters d and $2R$ as well as $d/2R$ were varied. The results are summarized in Fig. 8. In this figure, the abscissa shows the value of d for each simulation, while the maximal stresses in the weld detail are plotted on the vertical axis. The values of the parameters d and R are chosen in such a way that for various values of the ratio d/R at least one calculation for R taking the values 0.50, 0.75, 1.00 and

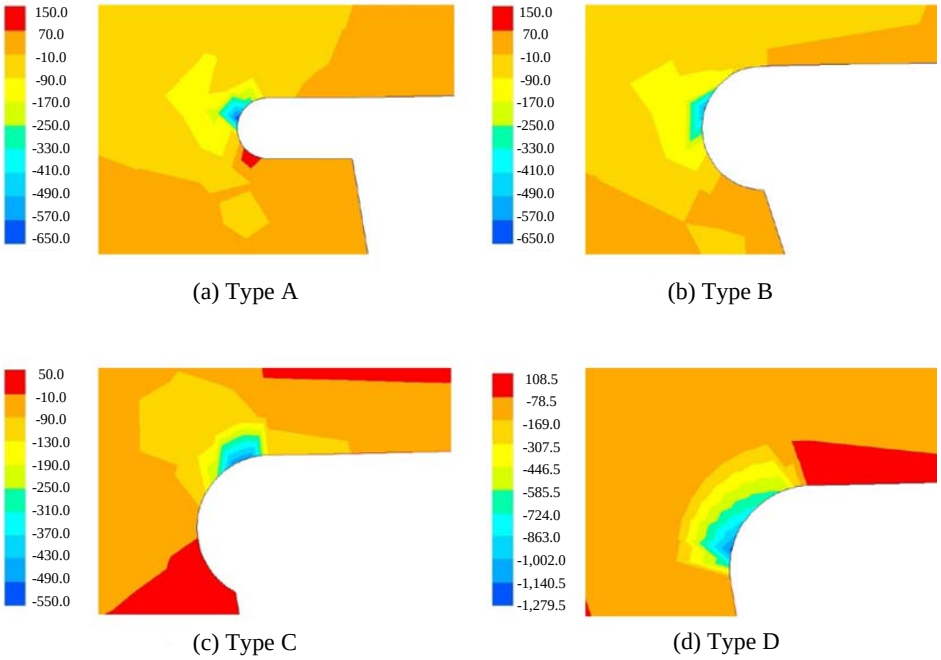

Fig. 7 Comparison of the transversal stresses in the different weld types.

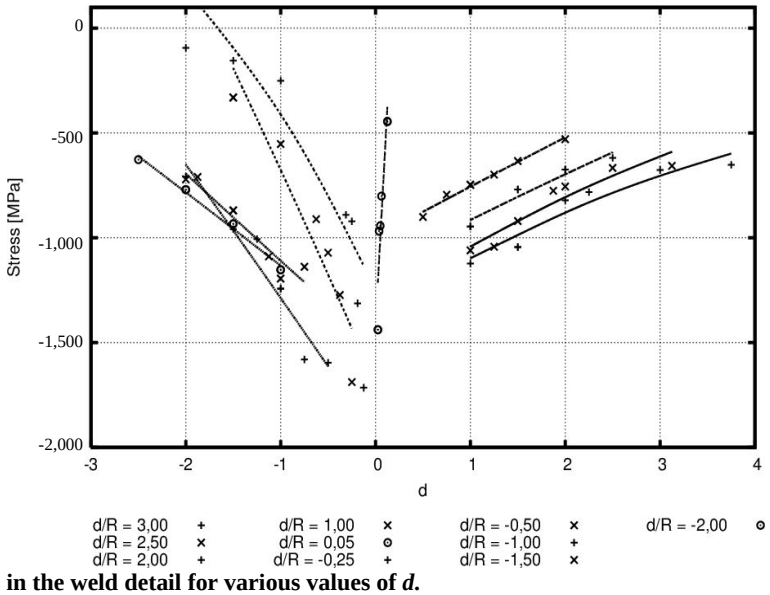

Fig. 8 Maximal stresses in the weld detail for various values of *d*.

1.25 and for *d* equalling 1.0, 1.5 and 2.0. If the identical values and unrealistic combinations of *d* and *R* are removed from the calculations, seventy stress values remain in the diagram in Fig. 8. Because of the large scattering of the stress values corresponding to parameters describing the weld, it is impossible to perform all calculations with exactly the same element geometry. Nevertheless, special attention was paid to ensure that all results remain comparable. Since all of the discussed trends can clearly be noticed from Figs. 8 and 9, it can be assumed that this endeavour was successful. Results of some calculations deviating from the regression curve can be attributed to this phenomenon. The points are grouped as a function of the weld type. The following conclusions can directly be derived from Fig. 8:

(1) A clear boundary appears to exist between the stress values of “Types A and B” for positive values

of *d* on the one hand, and "Types C and D" for negative values of *d* on the other hand;

(2) The stresses for positive values of *d* are obviously lower when compared to results for negative values of *d*, the latter not really showing lack of weld penetration;

(3) Higher values of *d*/*R* result in considerably higher stresses for "Types A, B and C". For these weld types, an increase of the ratio *d*/*R* results in larger cavity at the backside of the weld;

(4) The exception to the previous rule is "Type D". For a constant value of *d*, higher values of *R* apparently result in lower stress values. The transition between the web of the longitudinal stiffener and the deck plate is smoother for this specific weld type;

(5) For positive values of *d*, being "Types A and B", the following rules apply: increasing the depth *d*, lowers the stress level; increasing of the ratio *d*/*R*, also rises the stresses;

(6) As the ratio *d*/*R* takes a value close to 0, the trend line which can be constructed through results having the same value of *d*/*R* becomes steeper. Because of this fact and in contrast with the previous conclusion, extremely small values of the ratio *d*/*R* will still result in large stresses. The cavity of the lack of weld penetration shares some similarities with a crack in the weld material in this specific case, thus explaining this trend;

(7) For negative values of *d*, being "Types C and D", the following can be concluded: low values of *d*, result in low stresses; large values of *d*/*R* results in higher stresses will be, although some restrictions can be made concerning this rule;

(8) The closer *d*/*R* near to 0 from the negative side, the steeper the trend line of the results appears. For negative values of *d*, all trend lines for constant ratio *d*/*R* are noticeably steeper, thus emphasizing the effect for positive values of *d*.

Fig. 9 displays the calculation results, although grouped for each weld type, the abscissa now represents *R*. Both diagrams clearly demonstrate a second order relation between the radius *R* and the stress values. The inclination of the parabolic curve is much steeper for "Type C" and "Type D", as shown in Fig. 9b. Comparing both diagrams obviously shows that weld details with smaller lack of weld penetration (Fig. 9a) imply lower stress values than those details which have large lack of penetration (Fig. 9b).

The exact location of the stress concentrations has equally been compared as a function of the parameters previously identified. A circular section models the cavity of the lack of weld penetration in each finite element model of the parametric study. The length of the circular section varies from approximately a 45^{o} sector for "Type D" to a 180^{o} sector for "Type A" and "Type B". The location of the stress peak in the cavity

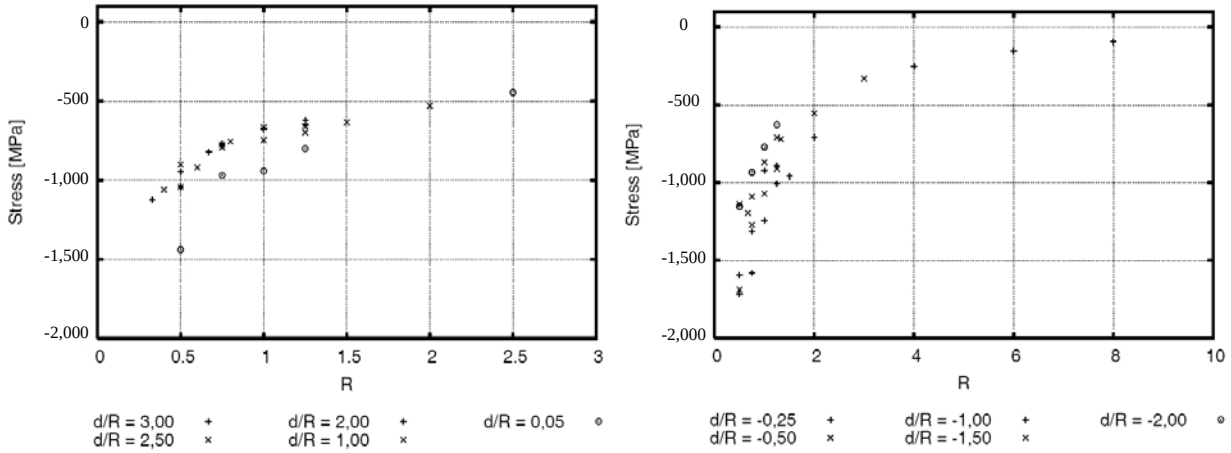

(a) "Type A" and "Type B" (b) "Type C" and "Type D"

Fig. 9 Maximal stresses in the weld detail for various values of *R*.

can be identified by its position on the normalised arc length of this circular section. A curvilinear coordinate is assumed, having its origin at the intersection of the circular section and the deck plate surfaces. The total length of the circular section is assumed to be 1, so all curvilinear coordinates vary between 0 and 1, although the actual length of the section will vary when comparing different simulations. Using this relative coordinate, the stress peak for "Type D" always seems to occur at the same coordinate of 0.87. For "Type C", the coordinate changes to a value of 0.46, a value which remains almost constant for "Type B" as well as for "Type A". The stress peak is always situated at the end of the cavity which is the zone where the curvature of the circular section representing the weld filet reaches its largest value. Hence, the location of the maximal stresses is invariable and slightly pointed in the direction of the deck plate.

Still, some caution is necessary when looking at the height of the stress values derived from a purely elastic calculation model such as this. An actual elasto-plastic calculation model would probably result in stresses which are more according to the situation in an actual bridge deck. Although the stress values in such a calculation would be less extreme, the zone where these stresses occur would be more or less similar. Unfortunately, such a calculation would require computer capacity in excess of what is available at this moment. Since only results of an elastic calculation are available, Fig. 10 displays a cross section of the weld for "Type C" and "Type D", wherein only the stresses lower than 250 MPa are drawn. The "stress peak zone" is defined as the area wherein stresses due to a purely elastic calculation exist which are higher than this value. A "stress peak zone" such as this can be defined for each of the weld details within this parametric analysis. In Fig. 11, these results are synthesised in one illustration for a constant value of R, equalling 1 mm and a variable depth d. This diagram clearly illustrates the evolution of the "stress peak zone" with the depth of the lack of weld penetration. The zone is generally located at the top part of the cavity edge and can be characterized by a slight bulge extending towards of the deck plate rather then to the stiffener web.

When varying from "Type A" to "Type D", the following changes of the "stress peak zone" occur:

(1) For "Type A", characterized by a large depth d, the "stress peak zone" is located in the upper part of the cavity, pointing slightly to the upper surface of the deck plate as well as to the exterior of the trapezoidal stiffener. Since the effective thickness of the stiffener web is reduced considerably for this weld type, high stresses appear in the remaining part of the stiffener web, which results in the second bulge of the "stress peak zone";

(2) As the weld evolves to "Type B" and "Type C", the effective width of the connection between the stiffener web and deck plate becomes more substantial.

(a) "Type C" (b) "Type D"

Fig. 10 "Stress peak zone" in the stiffener web to deck plate connection.

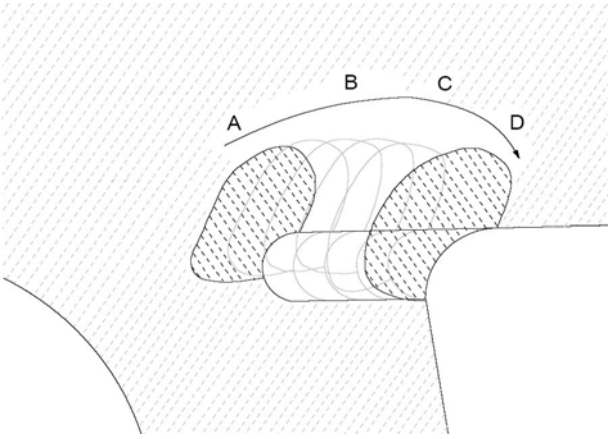

Fig. 11 Variation of the "stress peak zone".

Hence the "stress peak zone" will not be pointing to the outside of the stiffener web as was the case for "Type A". The bulge in the direction of the deck plate becomes slightly larger, the "stress peak zone" having moved towards the deck plate;

(3) Finally in the situation of "Type D", the contact length reaches a maximum size and encompasses the entire length of the arc between deck plate and stiffener web. In addition, the "stress peak zone" is clearly pointed in the direction of the deck plate.

As a conclusion and disregarding the case of an extremely large lack of weld penetration, the "stress peak zone" is clearly pointing towards the deck plate. Adding this to the location of the maximum stresses, it must be implied that possible fatigue cracks will be directed towards the deck plate and not to the stiffener web.

7. Conclusions

Although a considerable number of specimens, a total of 126, were examined, extrapolating these results to the connection between the stiffener web and the deck plate in general requires caution. This is because of the relatively small size of the considered batch, the limited number of steel fabricators and the fact that a single type of geometry of the longitudinal stiffeners was examined. Nevertheless, some trends can be derived from the study of the microscopic images of the lack of weld penetration.

Although the fabricators have been asked to guarantee a minimum of 80% penetration of the welding, it must be implied that an important dispersion exists of this parameter, in accordance with independent international research [12]. Notwithstanding the fact that all of the specimens were constructed with the utmost care and although they were all welded with the explicit purpose of performing a qualitative study of the considered weld detail, a considerable number of the specimens possesses a full penetration weld or even an excess of weld material.

Without naming definite percentages, it can be concluded that the required weld quality can not be assured, which has considerable consequences on the stresses in the weld. Since most orthotropic plated bridge decks include several meters of comparable welding, such decks will certainly suffer from less than optimal welding in a number of points of the orthotropic plated bridge deck. The bridge across the Albert Canal, mentioned previously in this paper, has a total length of 2,300 m of stiffener web to deck plate welds, while the bridge itself is only 115 m long. For applications of orthotropic plated sections in steel box girder bridges, this weld length will be even more substantial.

The weld detail being considered is subjected to extremely high stresses. For cases where a lack of weld penetration remains, larger values of d/R introduce higher stresses, d remaining constant. Alternatively, if d becomes very small, the stresses will rise equally.

The size as well as the shape of the stress peaks indicate that possible fatigue cracks for orthotropic plated bridge decks using a comparable geometry will be directed to the deck plate, except for those weld details which are suffering from insufficient weld penetration. The most precarious situation occurs for a small value of the radius R and small gap depths d and for weld details with an excessive amount of weld materials.

However, the actual weld finishing is not as smooth as has been assumed for the finite element modelling. Small deviations, sharper angles or micro-cracks may have a substantial influence on the size and shape of the stress peaks and the possible cracks. However, the conclusions presented above presumably hold as overall trends.

Another important factor for the fatigue behaviour will be the influence of residual stresses, which will also be dependent on d and d/R. This will be the subject of ongoing research.

References

[1] P.V. Bogaert, Fatigue resistance of a steel railway bridge, in: Proceedings of IABSE International Symposium on Durability of Structures, Lisbon, Portugal, 1989.

[2] P.V. Bogaert, Three steel arch bridges crossing the Brussels-Charleroi Canal—Design and construction, Stahlbau 68 (6) (1999) 409-419.

[3] P.V. Bogaert, Steel tied arch railway bridge, Louvain, Belgium, Struct. Eng. Int.—J. of IABSE 13 (1) (2003) 22-24.

[4] H.D. Backer, B.D. Pauw, W.D. Corte, P.V. Bogaert, Field testing of dispersion layers to reduce fatigue damage in orthotropic steel bridge decks, in: Proceedings of 4th Eurosteel Conference, Maastricht, The Netherlands, June 2005.

[5] H.D. Backer, Optimisation of the fatigue behaviour of the orthotropic plated bridge deck concept through better dispersion of traffic loads, Doctoral Thesis, Ghent University, Belgium, 2006. (in Dutch)

[6] EN1993-1-1, Eurocode 3: Design of Steel Structures—Part 1-1: General Rules and Rules for Buildings, European Committee for Standardization CEN, Brussels, 2005.

[7] EN1993-2, Eurocode 3: Design of Steel Structures—Part 2: Steel Bridges, European Committee for Standardization CEN, Brussels, 2006.

[8] W.D. Corte, P.V. Bogaert, H.D. Backer, Efficiency of closed stiffener orthotropic deck panels for railway bridges, Bridge Structures 1 (3) (2005) 203-209.

[9] L. Frýba, L. Gajdos, Fatigue properties of orthotropic decks on railway bridges, Engineering Structures 21 (7) (1999) 639-652.

[10] P.A. Tsakoupolos, J.W. Fisher, Full-scale fatigue tests of steel orthotropic deck panel for the Bronx-Whitestone Bridge rehabilitation, Bridge Structures 1 (1) (2005) 55-66.

[11] G. Opriessnig, M. Kettler, G. Beer, Elimination the influence of the mesh geometry to the quality of global smoothing, in: Proceedings of 5th International Conference on Information Visualisation, USA, 2001.

[12] P.A. Tsakoupolos, J.W. Fisher, Fatigue performance and design refinements of steel orthotropic deck panels based on full-scale laboratory tests, Int. J. Steel Struct. 5 (3) (2005) 211-223.